Supporting Information

One Building Block, Two Different Nanoporous Self-Assembled Monolayers: a Combined STM and Monte Carlo Study

Jinne Adisoejoso[1], Kazukuni Tahara[2], Shengbin Lei[3], Paweł Szabelski[4]*, Wojciech Rżysko[5], Koji Inukai[2], Matthew O. Blunt[1], Yoshito Tobe[2]*, Steven De Feyter[1]**

[1] Department of Chemistry, Division of Molecular Imaging and Photonics, Laboratory of Photochemistry and Spectroscopy, Katholieke Universiteit Leuven (KULeuven), Celestijnenlaan 200 F, B-3001 Leuven, Belgium, [2] Division of Frontier Materials Science, Graduate School of Engineering Science, Osaka University, Toyonaka, Osaka 560-8531, Japan, [3] Key Laboratory of Microsystems and Microstructures Manufacturing, Ministry of Education, Harbin Institute of Technology, Harbin, 150080, P. R. China, [4] Department of Theoretical Chemistry, Maria-Curie Skłodowska University, Pl. M.C. University, 3, 20-031 Lublin, Poland, [5] Department for the Modeling of Physico-Chemical Processes , Maria-Curie Skłodowska University, Pl. M.C. University, 3, 20-031 Lublin, Poland.

Email: leisb@hit.edu.cn, szabla@vega.umcs.lublin.pl, tobe@chem.es.osaka-u.ac.jp, Steven.DeFeyter@chem.kuleuven.be

A. Details of Monte Carlo Simulations and Additional STM Images

A.1. Additional Monte Carlo Simulations data

Under the conditions assumed in the preliminary CMC simulations, that is at very low adsorbate densities and temperatures and without solvent molecules in the system, formation of patterns *p*6 (A) and *p*2 (B) is nearly equally probable, with a slight preference for the *p*2 structure. For example, separate simulations showed that out of 500 independent assemblies 262 had the *p*2 structure. These results are shown in Figure S1, in which we plotted changes in the number of observed structures *p*6 (A) and *p*2 (B) during the simulation. Structural and energetic parameters of the ordered networks obtained in the simulations are summarized in Table S1.

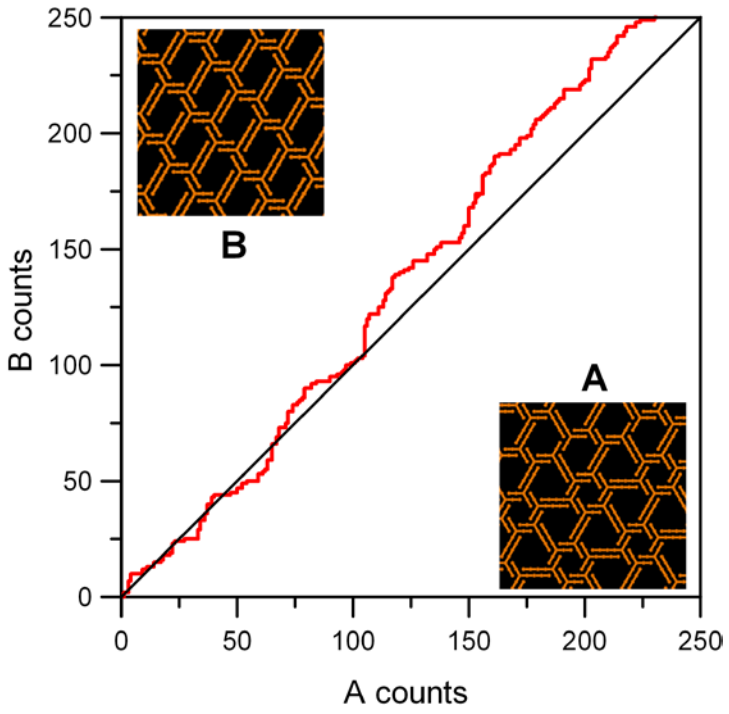

Figure S1. Changes in the number of observed structures *p*6 (A) and *p*2 (B) during the CMC simulation consisting of 500 independent runs. These results were obtained for 200 molecules of **DBA1** adsorbed on a 200 by 200 triangular lattice ($\rho = 0.045$), for $\varepsilon = -1$ and $T = 1.00$.

Table S1. Structural and energetic parameters of the ordered networks obtained in the simulations. The dimensions of the unit cells are in lattice constant units. The adsorbate density, ρ was defined as the average number of segments per one lattice site, that is $9N/L^2$ where N is the number of adsorbed **DBA1** molecules.

Structure	A	B	C
Unit cell shape and parameters	rhombic $a=\sqrt{97}$	parallelogram $a=\sqrt{43}$, $b=\sqrt{21}$, $\alpha=63.30^{\circ}$	parallelogram $a=2\sqrt{13}$, $b=3$, $\alpha=73.90^{\circ}$
Number of molecules per unit cell	6	2	2
Density	0.5567	0.5806	0.7500
Mean potential energy per molecule	12.5ε	12.5ε	12.0ε

To explore the phase coexistence in the adsorbed overlayer at higher densities, that is at $\rho\in\langle 0.4, 0.56\rangle$ we performed CMC simulations combined with the Parallel Tempering technique.[1] This allowed us to sample phase space of the system in an efficient way and to minimize the risk of trapping in metastable states. The simulations aiming at the determination of the topology of the phase diagram were performed on a 186 by 186 triangular lattice assuming periodic boundary conditions in both directions. For the sake of convenience the energy of interaction between the surface and a **DBA1** molecule was assumed to be equal to 0. Development of the porous superstructures from Figure 1c during the simulation was traced using the order parameter, *S*, which is related to mean tail-core distance in the adsorbed layer. Precisely, $S\in\langle 0,1\rangle$ is the fraction of molecules for which the distance between the terminal segment of the four-membered (long) arm and the core of a neighboring molecule measured in the direction of the long arm is equal to *d*. The meaning of the distance *d* is explained

graphically in the top part of Figure S2. Note that for the *p*6 structure (A) and *p*2 structure (B) *d* is equal to 5 and 7 lattice units, respectively, which allows for precise identification of each pattern.

Figure S2 shows the effect of temperature on the order parameter *S* corresponding to $d=7$, that is to the *p*2 structure (B).

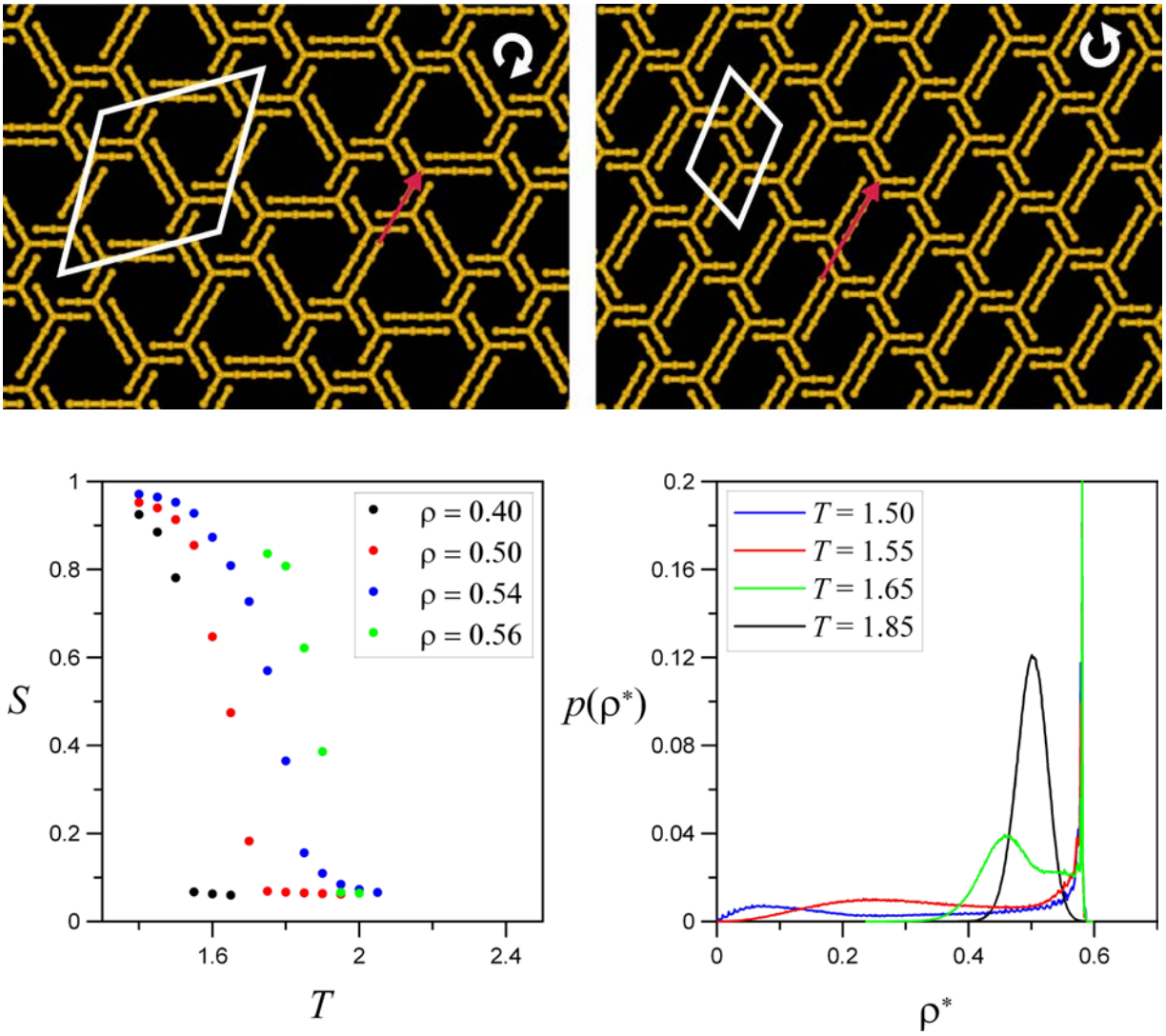

Figure S2. Small fragments of the *p*6 structure (A) and *p*2 structure (B). The thick white lines in the bottom part represent the corresponding unit cells, and the white arrow indicates the rotational direction of the pore. The red arrow shows the tail-core distance, *d* used in the definition of the order parameter *S*

(see text for details) (top). The order parameter *S* as a function of temperature, calculated for the *p*2 pattern (B), for the adsorbate densities ρ indicated in the figure (left). The block density probability distributions simulated for the temperatures shown in the figure (right). The results from the right part correspond to a system in which the adsorbate density was equal to 0.5 (bottom).

At sufficiently low temperatures *S* is very close to 1, which means that the entire system is filled with the *p*2 structure (B), regardless of the adsorbate density. With increasing temperature *S* drops to zero indicating that the *p*2 structure (B) vanishes and turns into disordered phase – 2D gas. This was confirmed by the observation of the associated values of the *S* parameter corresponding to phases *p*6 (A) and linear (C) ($d=4$), both of which were close to zero under these conditions (results not shown). Note that the results plotted in the left part of Figure S2 provide rough estimation of the transition temperature at which the *p*2 (B)-2Dgas phase change occurs at a given adsorbate density. Namely these temperatures can be found by numerical differentiation of the curves from Figure S2, and they are equal to 1.55, 1.70, 1.85 and 1.95 for the increasing values of adsorbate density shown in the figure. Plotting these points on a density-temperature plane gives an estimation of the topology of the phase diagram. However, to construct the diagram we used a more accurate complementary technique called the block density distribution function analysis[2,3] in which we monitored local adsorbate density ρ^* within 62 by 62 blocks into which the lattice was divided. The obtained distribution function $p(\rho^*)$ is defined as the normalized probability that the adsorbed phase has density ρ^* within a block. In a single-phase system $p(\rho^*)$ is a single gaussian peak with maximum at the most probable density. With increasing number of coexisting phases the number of peaks increases appropriately. In the case of two-phase system the lower and upper critical density at a given temperature can be obtained directly from the position of the peak maxima. These data were used for the construction of the phase diagram for our system.

The right part of Figure S2 shows examples of the distributions $p(\rho^*)$ calculated for the system with the total adsorbate density, ρ equal to 0.5. As seen in the figure, at the highest temperature 1.85 the adsorbed phase is totally disordered, as it is characterized by one peak centered at 0.5. Upon lowering of the temperature the system begins to fluctuate between two states for which the common one is that with, $\rho^* = 0.58$ represented by the sharp peak, which we truncated for the clarity of presentation. This peak corresponds to the ordered *p*2 structure (B) and its position determines the upper critical density. Regarding the lower critical density, the peak maxima shift towards lower values as the temperature decreases and they determine onset of the 2Dgas-*p*2 (B) phase transition in the system at a given temperature. Analyzing the positions of the maxima at different total adsorbate densities and different temperatures enabled us to determine topology of the phase diagram of **DBA1** adsorbed on a triangular lattice. The proposed diagram is shown in Figure S3.

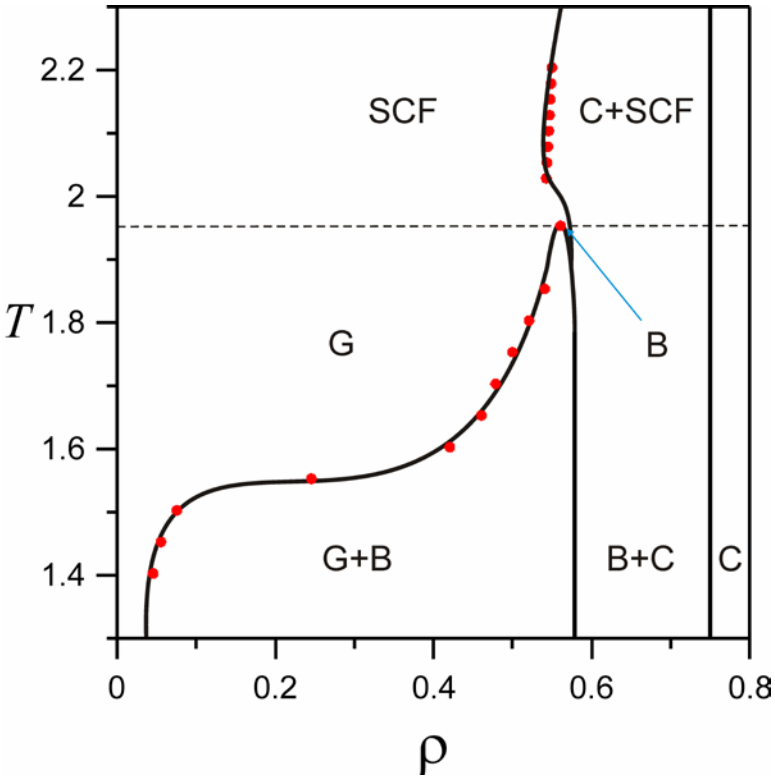

Figure S3. The phase diagram of **DBA1** on a triangular lattice. The letter codes G and SCF denote two-dimensional gas phase and supercritical fluid, respectively. The remaining symbols B and C correspond to the phases *p*2 and the linear packing. The red points are the simulated data and the vertical solid lines at 0.58 and 0.75 correspond to the density of an infinite defect-free pattern B and C respectively.

A.2. DBA1 in a mixture of *p*2 and *p*6 packings

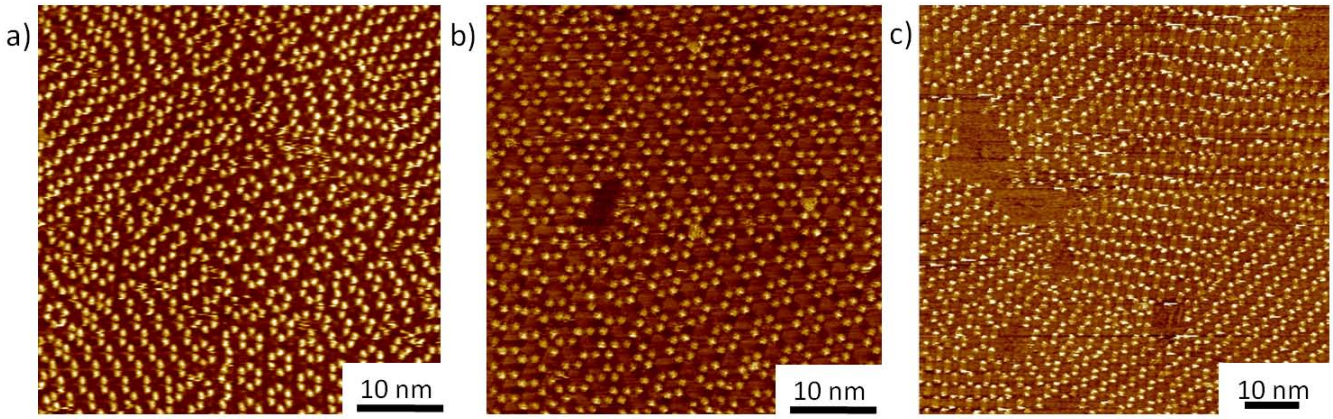

Figure S4. STM images of **DBA1** in a mixture of both porous packings *p*2 and *p*6 in a) TCB as a solvent at a ratio of 72/28 (*p*2/*p*6) at a concentration of 4.6×10^{-6} M and b) 1-Phenyloctane as a solvent at a ratio of 48/52 (*p*2/*p*6) at a concentration of 2.8×10^{-6} M c) 1-Octanoic acid as a solvent at a ratio of 94/6 (*p*2/*p*6) at a concentration of 3.0×10^{-6} M. (I_{set}: 0.1 nA, V_{set}: –1.0 V)

A.3. Tables with summarizing results

All the *p*2/*p*6 ratios are obtained by counting the area occupied by the *p*2 and the *p*6 structure out of 30 or more images of 80 × 80 nm² or more and then dividing this area by the total area (~200000 nm²) obtained from the 30 images. Both physical translations and scanner translations are used to avoid that the same area is measured twice. This method obtains an absolute value of the areas, therefore no error bar is given.

Table S2. Summary of Solvent Studies

Solvent	**~3 × 10^{-6} M (*p*2/*p*6)**
1,2,4-Trichlorobenzene	72/28
1-Octanoic Acid	94/6
1-Phenylhexane	52/48
1-Phenyloctane	48/52
1-Phenyldecane	56/44
1-Phenyldodecane	83/17
1-Phenyltetradecane	91/9

Table S3. Summary of Concentration Studies

1,2,4-Trichlorobenzene	**(*p*2/*p*6)**	**1-Phenyloctane**	**(*p*2/*p*6)**
4.6 × 10^{-6} M	72/28	2.8 × 10^{-6} M	48/52
3.1 × 10^{-6} M	69/31	1.4 × 10^{-6} M	18/82
2.3 × 10^{-6} M	71/29	6.9 × 10^{-7} M	0/100
1.9 × 10^{-6} M	69/31		

Table S4. Summary of Temperature experiments at a concentration of 4.6×10^{-6} M for TCB and 2.8×10^{-6} M for PO.

	1,2,4-Trichlorobenzene ***p*2/*p*6**	**1-Phenyloctane** ***p*2/*p*6/linear**
25 °C	72/28	48/52/0
30 °C	83/17	0/0/100
40 °C	100/0	0/0/100
50 °C	100/0	0/0/100

A.4. DBA1 at lower concentration.

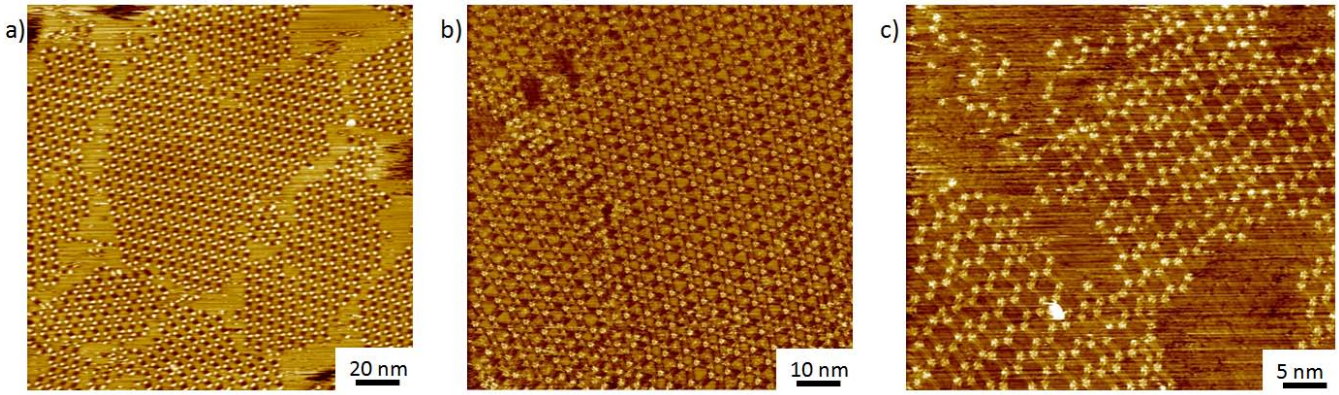

Figure S5. STM images of **DBA1** at a) the TCB/HOPG interface at low concentration (1.9×10^{-6} M) showing a mixture of *p*2 and *p*6 in a 69/31 ratio, b) the 1-phenyloctane/HOPG interface at low concentration (6.9×10^{-7} M) showing the unique formation of the *p*6 structure, c) the 1-octanoic acid/HOPG interface at low concentration (9.9×10^{-7} M) showing the unique formation of the *p*2 structure (I_{set}: 0.1 nA, V_{set}: –0.8 V)

A.5. Molecular model of 1-octanoic acid solvent molecules coadsorbed in the pore of the *p*2 structure

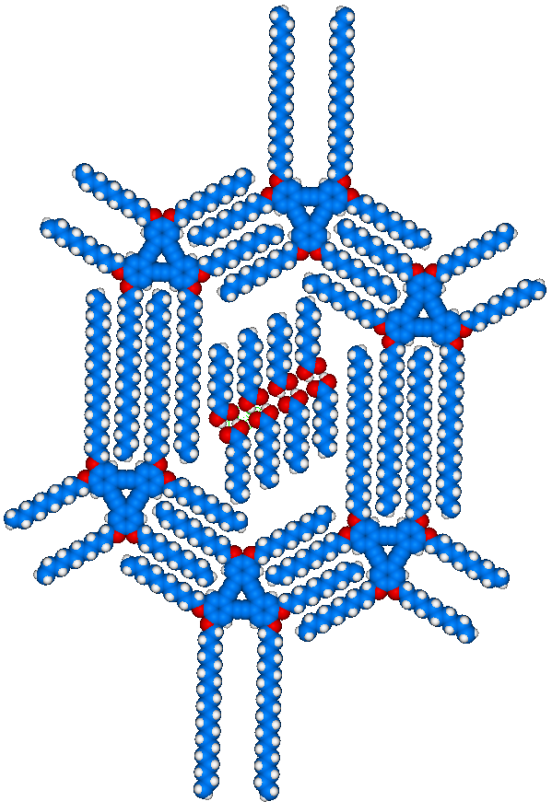

Figure S6. Molecular model of dimers of 1-octanoic acid molecules coadsorbed in the pore of **DBA1** in the *p*2 packing.

A.6. Temperature Experiments

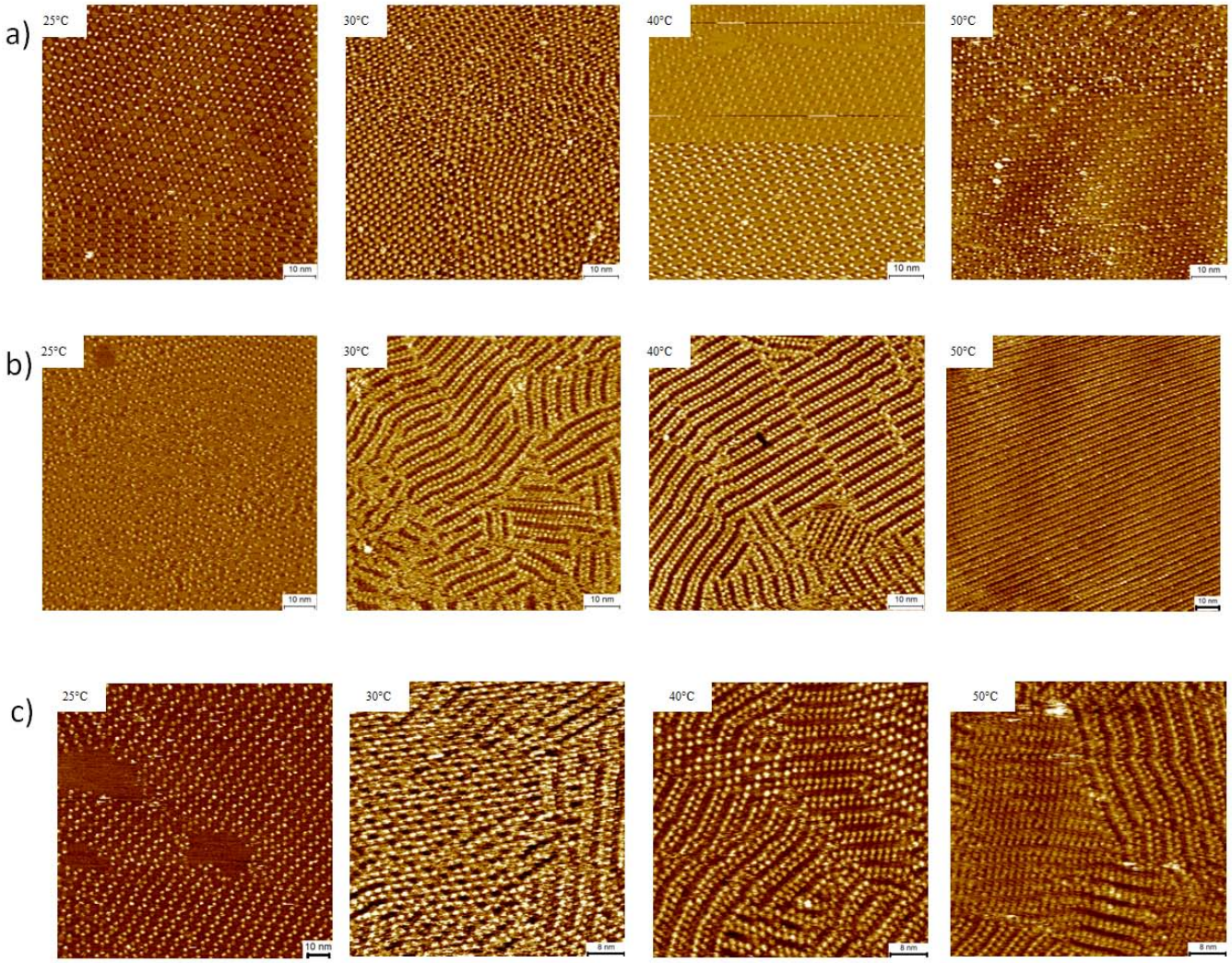

Figure S7. a) STM images of **DBA1** at the TCB/HOPG interface at different temperatures (indicated in the upper left). The ratio of the *p*2 and *p*6 network occurrence changes from 70/30 at room temperature to 100% *p*2 at 40-50 °C. b) STM images of **DBA1** at the 1-phenyloctane/HOPG interface at different temperatures (indicated in the upper left). The network changes from a mixture of *p*2 and *p*6 in a 50/50 distribution at room temperature to a complete coverage of the linear structure at higher temperatures (30-50 °C). (I_{set}: 0.1 nA, V_{set}: –0.8 V). c) STM images of **DBA1** at the 1-octanoic acid/HOPG interface at different temperatures (indicated in the upper left). The network changes from the *p*2 network to a mixture of *p*2 and linear at 30 °C and a complete linear packing at higher temperatures. (I_{set}: 0.1 nA, V_{set}: -0.8 V).

A.7. Large scale image of the four-component network

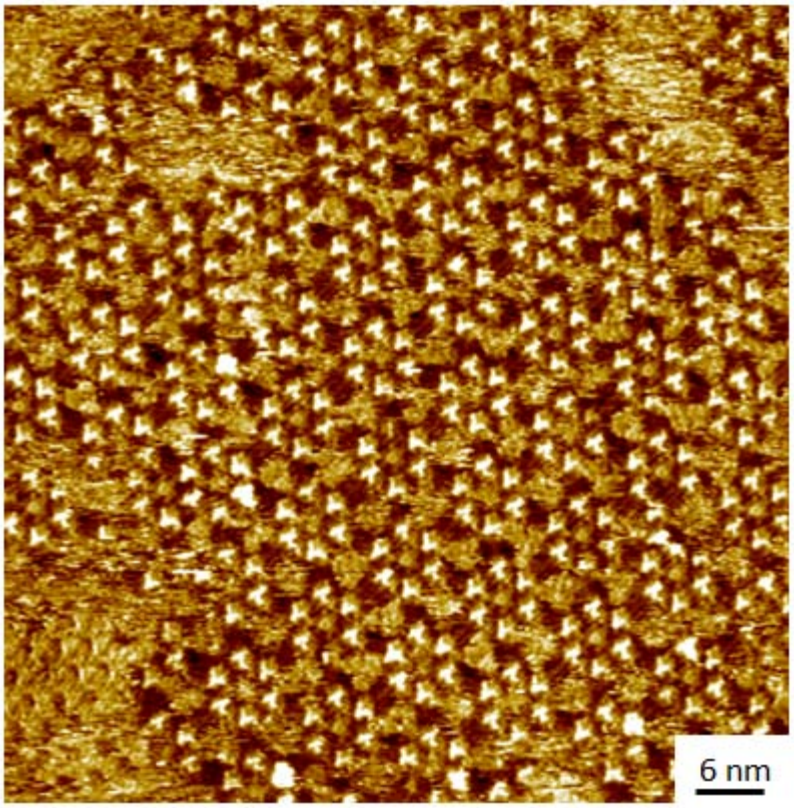

Figure S8. Large scale STM image of a monolayer of a monolayer of **DBA1** (6.9×10^{-7} M), **COR** (3.0×10^{-3} M), **ISA** (5.5×10^{-3} M) and **NG** (1.7×10^{-3} M) at the 1-phenyloctane/HOPG interface. Next to the four-component network, several domains of pure guest molecules can be found (lower left) as well as fuzzy domains, which can be attributed to mobile guests.

A. Synthesis of DBA1.

The synthesis of **DBA1** is outlined in Scheme S1.

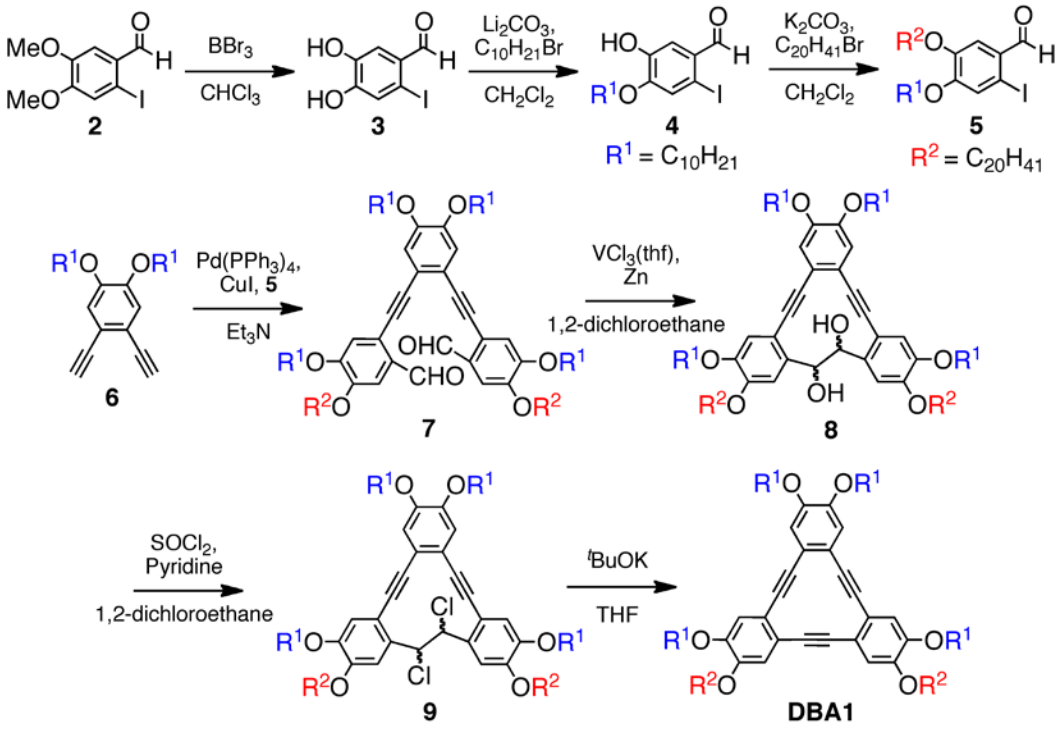

Scheme S1. Outline of the synthesis of **DBA1**

Experimental Section

General. All manipulations were performed in an inert gas (nitrogen or argon) atmosphere. All solvents were distilled before use. All commercially available reagents were used as received. $Pd(PPh_3)_4$,[4] **2**,[5] and **5**[6] were prepared following the literature.

^1H (400 MHz and 300 MHz) and ^{13}C (100 MHz and 75 MHz) NMR spectra were measured on a JEOL JNM AL-400 and a Varian Mercury 300 spectrometers, respectively. When chloroform-*d* and acetone-d_6 were used as solvents, the spectra were referenced to residual solvent hydrogen in the ^1H NMR spectra (7.26 ppm for chloroform-*d* and 2.05 ppm for acetone-d_6) and to solvent carbon in the ^{13}C NMR spectra (77.0 ppm for chloroform-*d* and 29.8 ppm for acetone-d_6), respectively. Other spectra were recorded by the use of the following instruments: IR spectra, JASCO FT/IR-410; Mass spectra,

JEOL JMS-700 for EI ionization mode and AXIMA-CFR for LD ionization mode. Elemental analyses were carried out with a Perkin-Elmer 2400II analyzer.

Synthesis of 3. To the solution of 2-iodo-4,5-dimethoxybenzaldehyde **2** (7.96 g, 26 mmol) in $CHCl_3$ (110 mL), BBr_3 (5.0 mL, 53 mmol) was add dropwise. After stirring for 17 h at room temperature, the reaction mixture was poured into the ice water. The products were extracted with ether, the organic phase was washed with water. After addition of sat. $NaHCO_3$ aq. to the aqueous phase, the aqueous phase was extracted with ether. The organic phases were combined, washed with sat. $Na_2S_2O_3$ and brine, dried over $MgSO_4$. After evaporation of solvents under vacuum, the product was purified by the use of silica gel column chromatography (hexane/AcOEt = 1/1) to afford **3** (6.6 g, 90%) as white solids; mp 169–171 ºC; ^{1}H NMR (300 MHz, acetone-d_6, 30 °C) δ 9.79 (s, 1H), 7.42 (s, 1H), 7.37 (s, 1H); ^{13}C NMR (75 MHz, acetone-d_6, 30 °C) δ 194.4. 153.3, 147.0, 128.8, 127.1, 116.5, 90.4; IR (KBr) 3491, 3051, 2985, 2931, 2692, 2585, 1649 cm^{-1}; Anal. calcd for $C_7H_5O_3I$: C, 31.84; H, 1.91; found: C, 32.23; H, 1.83.

Synthesis of 4. Diol **3** (1.83 g, 6.29 mmol) and Li_2CO_3 (7.29, 9.88 mmol) were suspended in DMF (30 mL). The mixture was stirred for 30 min at room temperature, then for 1 h to 45 °C. Solution of 1-boromodecane (2.18 g, 9.90 mmol) in DMF was added to the mixture. After stirring for 20 h at 45 °C, the reaction was quenched with the addition of sat. NH_4Cl aq., and the mixture was extracted with $CHCl_3$. The organic phase was dried over $MgSO_4$ and evaporated. The reside was purified by the silica gel column chromatography (hexane/chloroform/acetone = 14:5:1 as eluent) to give **4** (907 mg, 32%) as colorless crystals. mp 61.7–62.2 °C; ^{1}H NMR (300 MHz, $CDCl_3$, 30 °C) δ 9.85 (s, 1H), 7.46 (s, 1H), 7.28 (s, 1H), 5.79 (s, 1H), 4.10 (t, J = 6.6, 2H), 1.84 (quint, J = 6.6, 2H), 1.52–1.18 (m, 14H), 0.88 (t, J = 6.3, 3H); ^{13}C NMR (100 MHz, $CDCl_3$, 30 °C) δ 194.5, 151.5, 146.3, 128.8, 122.0, 115.2, 90.3, 69.7, 31.9, 29.5, 29.32, 29.30, 28.95, 25.9, 22.7, 14.2; IR (KBr) 3541, 3339, 3046, 2949, 2925, 2869, 2850, 1679, 1604, 1496, 1469, 1419, 1394, 1275, 1154, 1012, 996 cm^{-1}; HRMS (EI) calcd for $C_{17}H_{25}O_3I$ 404.0848, found 404.0833.

Synthesis of 5. Compound **4** (814 mg, 2.01 mmol), 1-bromoicoasne (1.09 g, 3.02 mmol), and K_2CO_3 (557 mg, 4.03 mmol) were suspended in DMF (10 mL). After stirring for 22 h at 60 °C, the reaction was quenched with the addition of sat. NH_4Cl aq.. The products were extracted with $CHCl_3$, and dried over $MgSO_4$. After removing the solvent under vacuum, the product was separated by the silica gel column chromatography (hexane/$CHCl_3$ = 4/1 as eluent) to afford **5** (1.26 g, 92%) as white solids. mp 67.1–67.9 °C; ^{1}H NMR (300 MHz, $CDCl_3$, 30 °C) δ 9.84 (s, 1H), 7.39 (s, 1H), 7.28 (s, 1H), 4.09–4.00 (m, 4H), 1.90–1.77 (m, 4H), 1.54–1.20 (m, 48H), 0.95–0.83 (m, 6H); ^{13}C NMR (75 MHz, $CDCl_3$, 30 °C) δ 194.7, 154.7, 149.6, 128.1, 123.1, 112.9, 92.4, 69.5, 69.2, 31.98, 31.96, 29.76, 29.71, 29.65, 29.62, 29.60, 29.41, 29.39, 29.35, 29.03, 28.97, 26.01, 25.95, 22.7, 14.2; IR (KBr) 3075, 2955, 2919, 2848, 1678, 1579, 1503, 1466, 1390, 1265, 1211, 1166, 1068, 1015, 977 cm^{-1}; HRMS (EI) calcd for $C_{37}H_{65}O_3I$ 684.3978, found 684.3967.

Synthesis of 7. Diethynylbenzene **6** (366 mg, 0.835 mmol), **5** (1.20 g, 1.75 mmol), $Pd(PPh_3)_4$ (49 mg, 42 μmol), and CuI (14 mg, 74 μmol) were suspended in Et_3N (50 mL). After stirring for 10 h at room temperature, the reaction was heated to 80 °C. After 2 h, the water and hexane were added to the mixture. The organic phase was washed with water and brine, and dried over $MgSO_4$. The purification was performed by the silica gel column chromatography (hexane/CH_2Cl_2 = 1/1 as eluent) to afford **7** (953 g, 76%) as yellow solids. mp 77.1–78.3 °C; ^{1}H NMR (400 MHz, $CDCl_3$, 30 °C) δ 10.56 (s, 2H), 7.36 (s, 2H), 7.02 (s, 2H), 6.99 (s, 2H), 4.09–4.02 (m, 8H), 4.01–3.94 (m, 4H), 1.92–1.77 (m, 12H), 1.53–1.21 (m, 124H), 0.92–0.86 (m, 18H); ^{13}C NMR (100 MHz, $CDCl_3$, 30 °C) δ 190.4, 153.8, 149.70, 149.65, 129.9, 121.2, 118.1, 116.0, 115.5, 109.7, 93.7, 88.0, 69.4, 69.22, 69.16, 32.0, 29.8, 29.71, 29.68, 29.63, 29.44, 29.41, 29.2, 29.11, 29.07, 26.06, 26.03, 22.7, 14.15; IR (KBr) 2922, 2851, 2206, 1683, 1591, 1515, 1468, 1371, 1286, 1230, 1146, 1098 cm^{-1}; MS (LD): m/z = 1552 [$(M+H)^+$].

Synthesis of 8. The solution of VCl_3 (228 mg, 1.45 mmol) in THF (5.0 mL) was refluxed for 21 h. Color of the reaction mixture was gradually changed from black to red. Upon cooling the reaction mixture to –78 °C, red colored precipitates were formed. After removing the THF via a syringe, the red

precipitates were washed with pentane several times and dried under vacuum. To the resulting pink colored solid, Zn (66.8 mg, 1.02 mmol), DMF (0.20 mL), and 1,2-dichloroethane (15 mL) were added. After being stirred for 30 min at room temperature, a solution of **7** (340 mg, 219 μmol) in 1,2-dichloroethane (6.0 mL) was added dropwise via a syringe at the rate of 2.0 mL/h to the mixture. After continuous stirring for 20 h, 10 wt% potassium (+)-tartrate aq. was added to the mixture, products was extracted with $CHCl_3$, and the organic phase was dried over $MgSO_4$. After evaporation of the solvents under vacuum, the product was separated by the silica gel column chromatography (hexane/$CHCl_3$ = 1/1 ~ 1/2 as eluent) to afford **8** (280 mg, 82%) as erythro isomer as brown sticky oil. ^{1}H NMR (300 MHz, $CDCl_3$, 30 °C) δ 7.32 (s, 1H), 7.18 (s, 1H), 7.09 (s, 1H) 7.01 (s, 1H), 6.97 (s, 1H), 6.93 (s, 1H), 5.52 (dd, *J* = 9.5, 3.0, 1H) 4.35 (t, *J* = 9.5, 1H), 4.17–3.78 (m, 12H), 3.41 (d, *J* = 9.5, 1H), 2.35 (s, 1H), 1.95–1.13 (m, 136H), 0.97–0.83 (m, 18H); ^{13}C NMR (100 MHz, $CDCl_3$, 30 °C) δ 150.5, 149.2, 149.1, 148.9, 148.2, 148.1, 139.0, 137.8, 118.8, 118.5, 118.4, 116.5, 115.4, 115.1, 114.4, 114.3, 111.3, 110.1, 94.2, 91.9, 91.6, 90.3, 82.3, 71.9, 69.6, 69.49, 69.30, 69.25, 69.21, 32.0, 29.76, 29.71, 29.69, 29.66, 29.64, 29.49, 29.46, 29.41, 29.37, 29.18, 29.14, 26.18, 26.13, 26.06, 26.04, 22.7, 14.2; IR (KBr) 3545, 2923, 2853, 2193, 1598, 1512, 1468, 1360, 1228 cm^{-1}; MS (LD): *m*/*z* = 1553 (M^+).

Synthesis of 9. Pyridine (25 μL, 0.31 mmol) and $SOCl_2$ (25 μL, 0.34 mmol) were added to a solution of **8** (135 mg, 86.8 μmol) in dichloroethane (1.5 mL). After stirring for 3 h at room temperature, the reaction was quenched with the addition of water. The products were extracted with CH_2Cl_2, washed with brine, and dried over $MgSO_4$. The solvents are removed under vacuum. The brown reside was subject to the silica gel column chromatography (hexane/CH_2Cl_2 = 4/1 ~ 3/2 as eluent) to give **9** (79 mg, 57%) as a mixture of stereoisomers (threo and erythro). Further careful separation by the silica gel column chromatography (same eluents) the mixture of stereoisomes gave threo isomer (25 mg, 18%) and erythro isomer (29 mg, 21%). Both isomers are brown sticky oil. (threo isomer); ^{1}H NMR (300 MHz, $CDCl_3$, 30 °C) δ 7.48 (s, 2H), 7.09 (s, 4H), 5.67 (s, 2H), 4.18–3.91 (m, 12H), 1.92–1.76 (m, 12H), 1.57–1.09 (m, 136H), 0.95–0.75 (m, 18H); ^{13}C NMR (100 MHz, $CDCl_3$, 30 °C) δ

149.3, 149.0, 148.6, 133.7, 118.7, 116.0, 115.6, 114.6, 112.5, 93.1, 90.1, 69.34, 69.27, 64.5, 32.0, 29.8, 29.7, 29.53, 29.47, 29.42, 29.33, 29.28, 26.1, 22.8, 14.2; IR (KBr) 2923, 2850, 1597, 1513, 1468, 1361, 1228, 1065 cm^{-1}; MS (LD): *m*/*z* = 1554 ($[M–Cl]^+$). (erythro isomer); ^1H NMR (300 MHz, $CDCl_3$, 30 °C) δ 7.22 (s, 1H), 7.20 (s, 1H), 7.10 (s, 1H), 7.05 (s, 1H), 7.02 (s, 1H), 7.00 (d, *J* = 11.3, 1H), 6.91 (s, 1H), 5.01 (d, *J* = 11.3, 1H), 4.15–3.91 (m, 12H), 1.91–1.75 (m, 12H), 1.58–1.10 (m, 136H), 0.96–0.77 (m, 18H); ^{13}C NMR (100 MHz, $CDCl_3$, 30 °C) δ 150.1, 149.17, 149.09, 148.9, 148.6, 135.1, 133.3, 119.5, 119.4, 118.5, 116.7, 116.3, 115.9, 114.7, 113.9, 113.3, 111.3, 95.1, 93.4, 90.7, 90.2, 69.44, 69.42, 69.37, 69.31, 69.2, 67.2 59.2, 32.0, 29.8, 29.71, 29.67, 29.65, 29.52, 29.50, 29.47, 29.41, 29.35, 29.27, 29.25, 29.21, 26.2, 26.13, 26.08, 26.07, 22.8, 14.2; IR (KBr) 2924, 2854, 1598, 1514, 1468, 1361, 1231, 1096, 1061 cm^{-1}; MS (LD): *m*/*z* = 1554 ($[M–Cl]^+$).

Synthesis of DBA1. To a suspension of ^{t}BuOK (20.6 mg, 184 μmol) in THF (0.3 mL), a solution of chloride **9** (29.3 mg, 18.4 μmol) in THF (0.5 mL) was added. After stirring for 2 d at 50 °C, the solvent was removed under vacuum. The mixture was purified by the silica gel column chromatography (CH_2Cl_2/hexane = 1/4 as eluent) and recrystalized from CH_2Cl_2/MeOH to afford **DBA1** (21 mg, 75%) as yellow solids. mp 66.5–68.2 °C; ^1H NMR (400 MHz, $CDCl_3$, 30 °C) δ 6.72 (s, 6H), 4.00–3.84 (m, 12H), 1.88–1.72 (m, 12H), 1.52–1.20 (m, 124H), 0.98–0.82 (m, 18H); ^{13}C NMR (100 MHz, $CDCl_3$, 30 °C) δ 149.1, 119.8, 115.9, 91.8, 69.1, 31.99, 31.97, 29.8, 29.71, 29.69, 29.66, 29.62, 29.43, 29.39, 29.2, 26.1, 22.7, 14.2; IR (KBr) 2919, 2850, 2206, 1593, 1510, 1470, 1351, 1228, 1071, 1016 cm^{-1}; Anal. calcd for $C_{104}H_{172}O_6$: C, 82.26; H, 11.42; found: C, 82.11; H, 11.03.

NMR Spectra of All New Compounds.

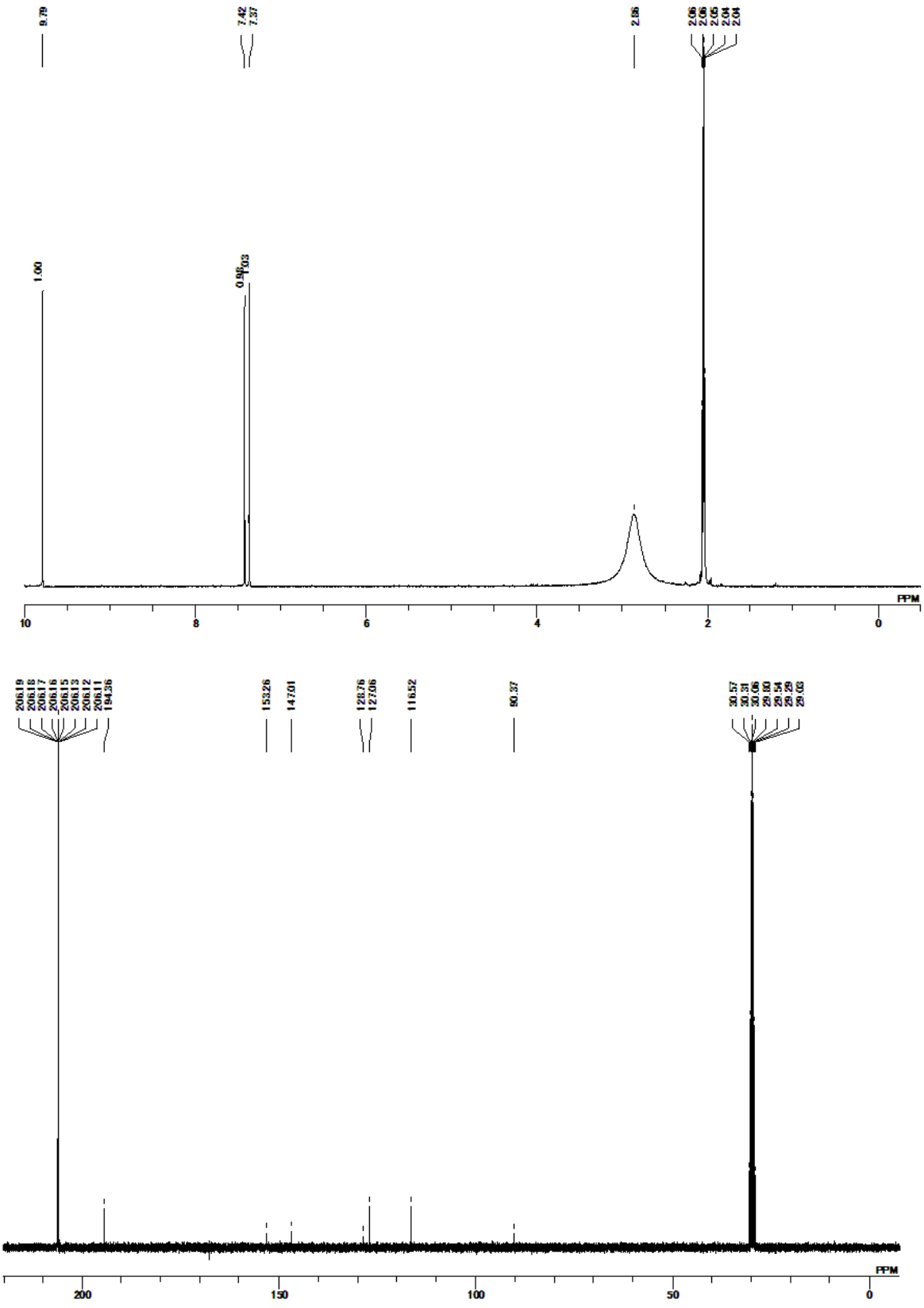

Figure S9. ^{1}H (upper) and ^{13}C (lower) NMR spectra of **3** in acetone-d_6 at 30 °C.

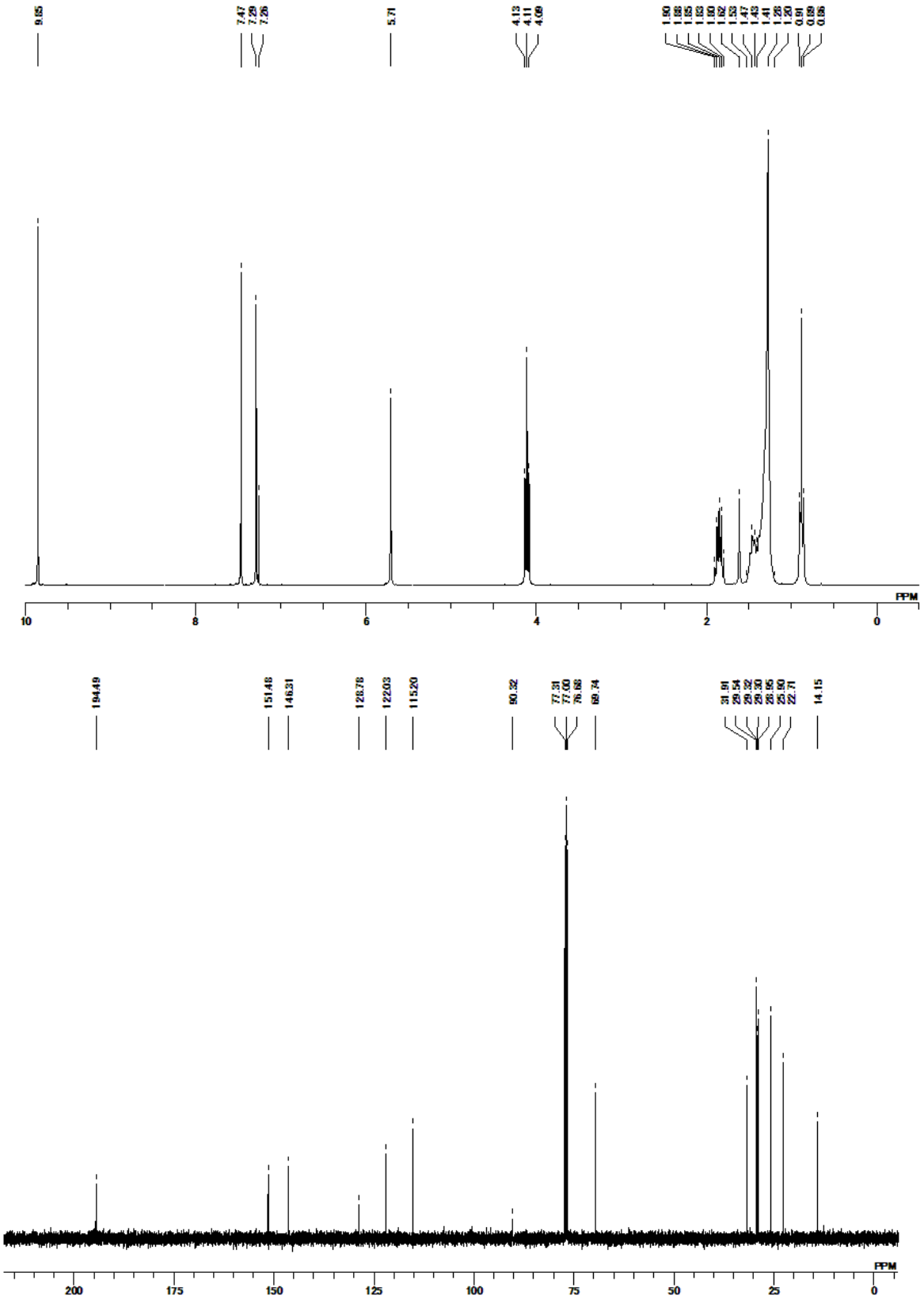

Figure S10. ^{1}H (upper) and ^{13}C (lower) NMR spectra of **4** in $CDCl_3$ at 30 °C.

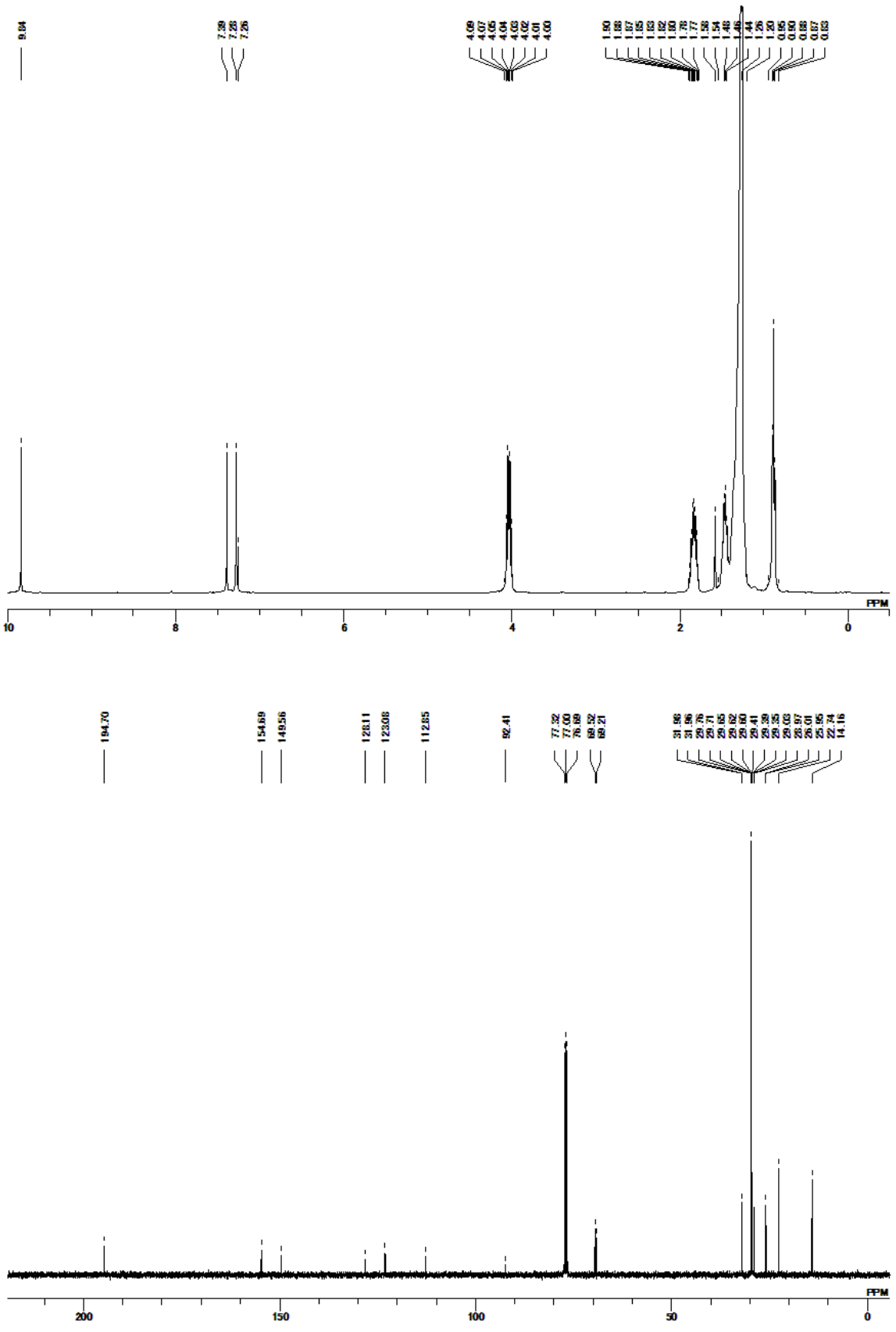

Figure S11. ^{1}H (upper) and ^{13}C (lower) NMR spectra of **5** in $CDCl_3$ at 30 °C.

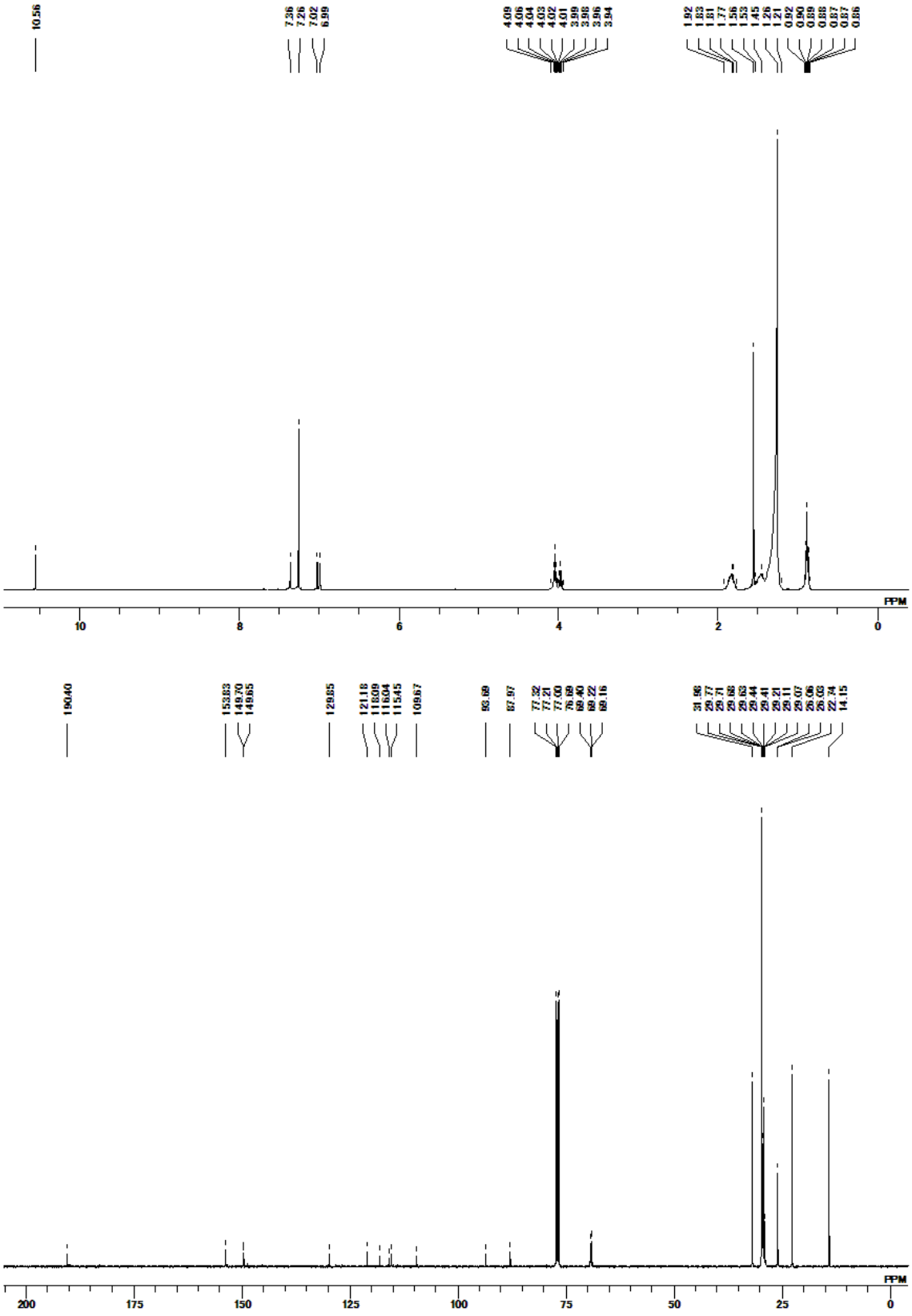

Figure S12. ^{1}H (upper) and ^{13}C (lower) NMR spectra of **7** in $CDCl_3$ at 30 °C.

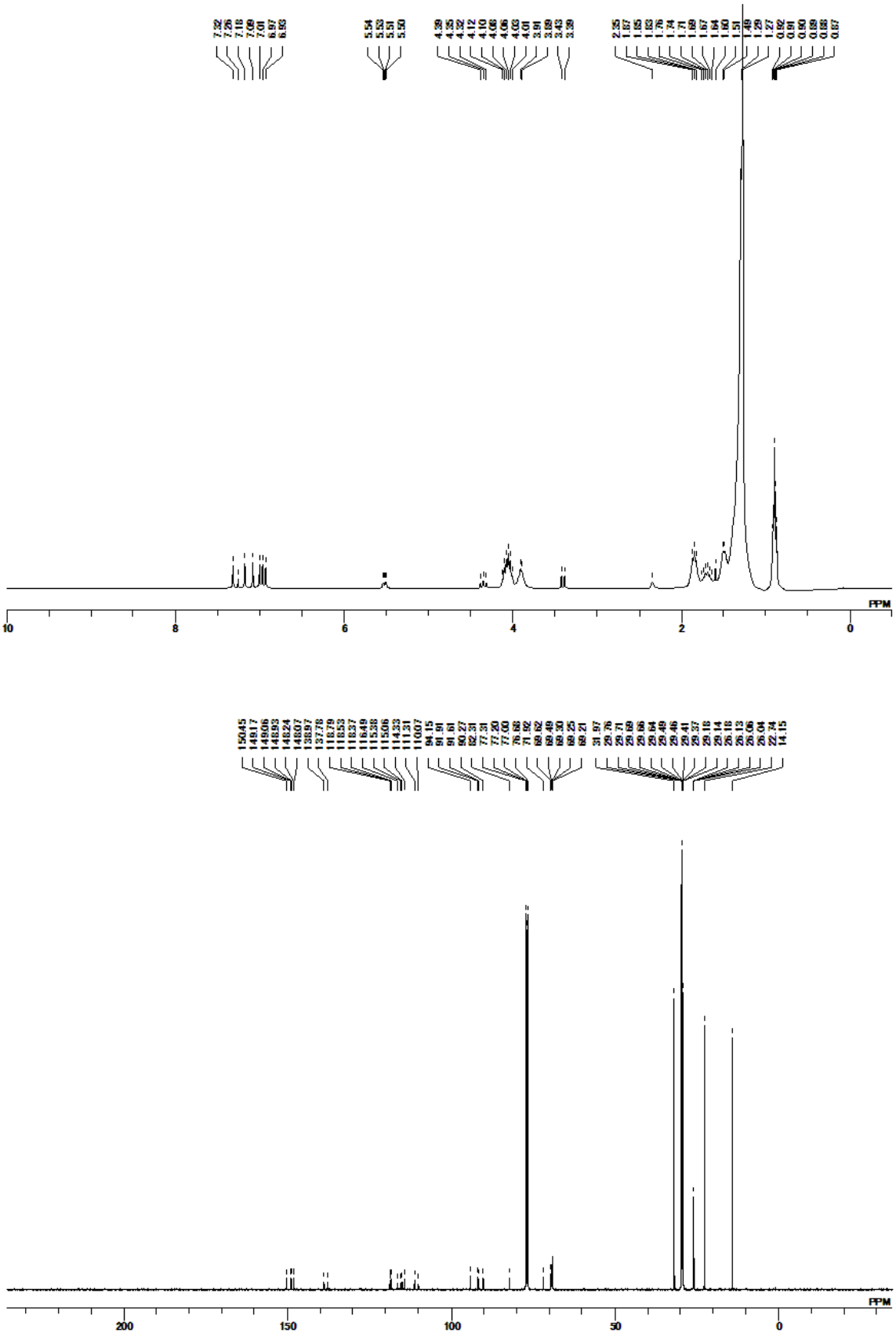

Figure S13. ^{1}H (upper) and ^{13}C (lower) NMR spectra of **8** in $CDCl_3$ at 30 °C.

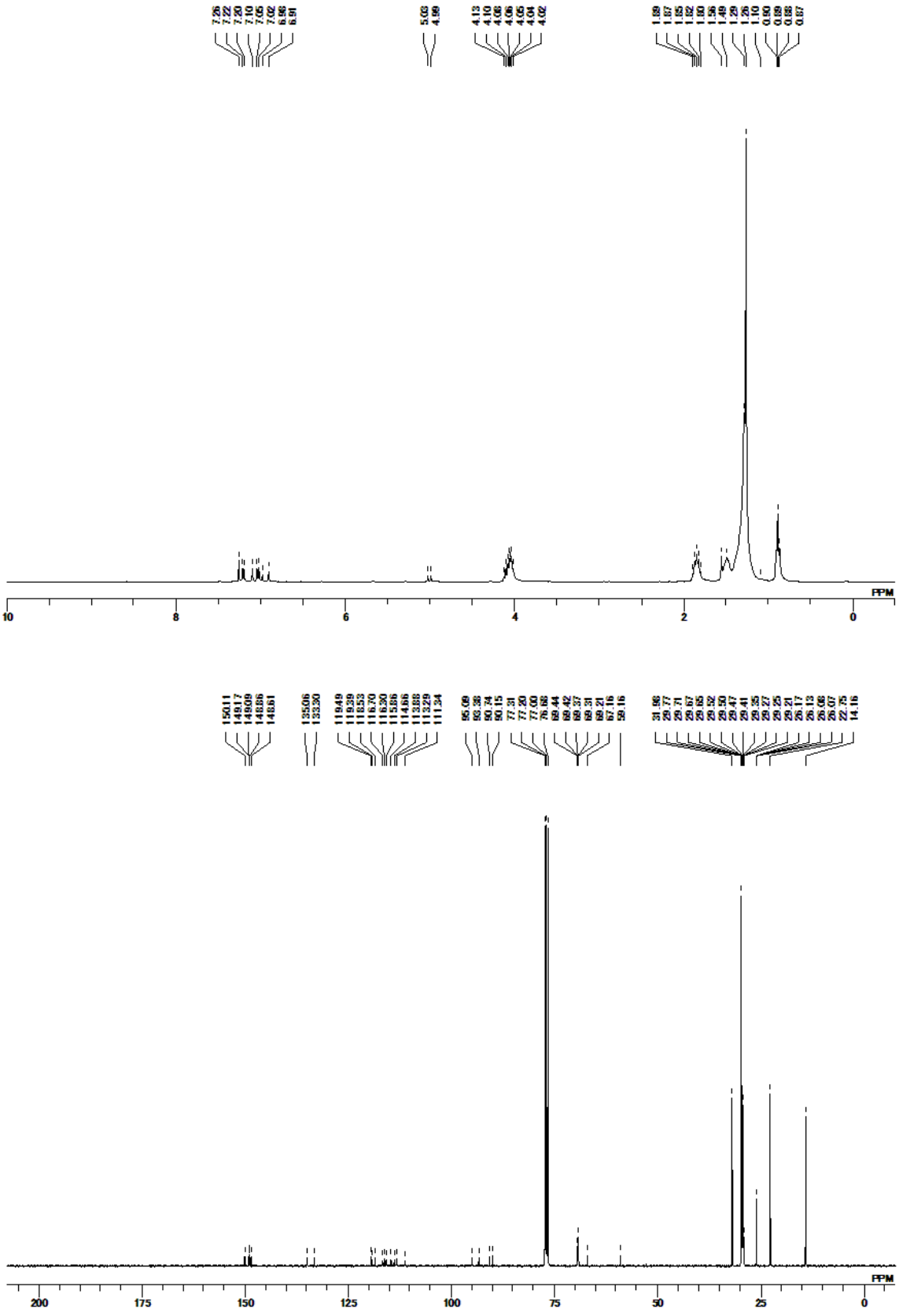

Figure S14. ^{1}H (upper) and ^{13}C (lower) NMR spectra of **9** (erythro) in $CDCl_3$ at 30 °C.

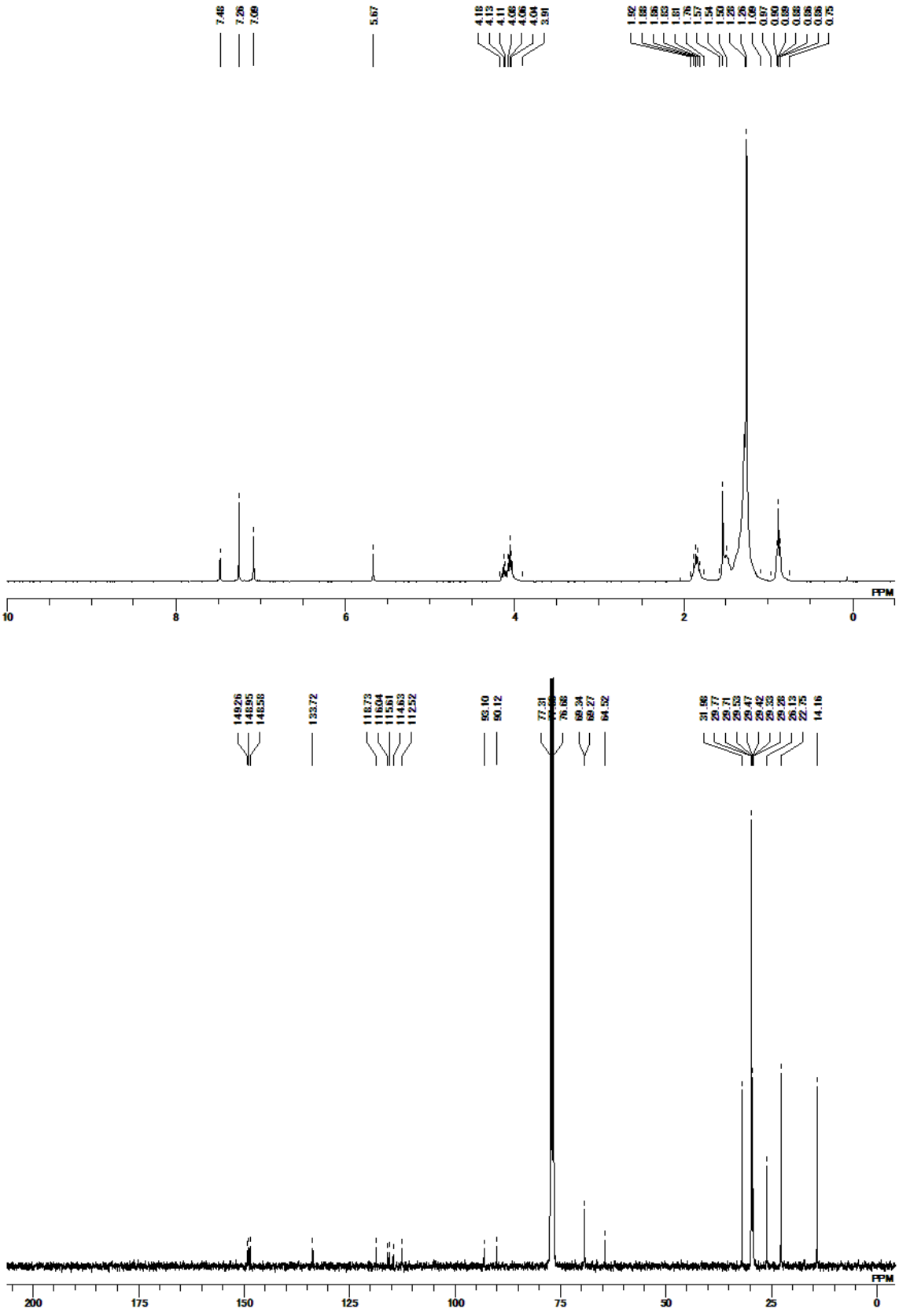

Figure S15. ^{1}H (upper) and ^{13}C (lower) NMR spectra of **9** (threo) in $CDCl_3$ at 30 °C.

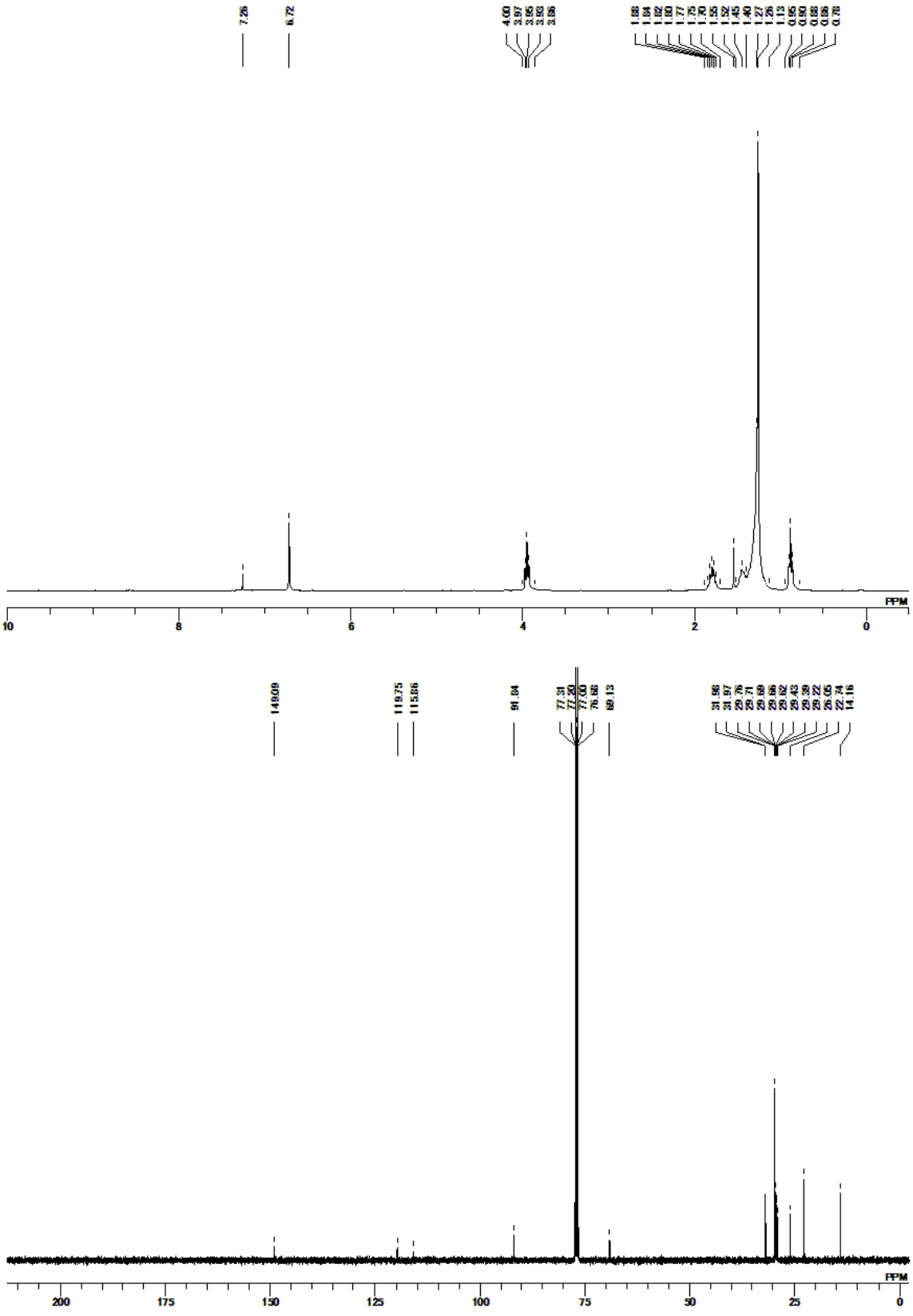

Figure S16. ^{1}H (upper) and ^{13}C (lower) NMR spectra of **DBA1** in $CDCl_3$ at 30 °C.

C. References

(1) de Pablo, J.J. ; Yan, Q. ; Escopedo, F.A. Simulation of Phase Transitions in Fluids. *Annu. Rev. Phys. Chem.* **1999,** *50*, 337-411.

(2) Binder, K. Finite Size Scaling Analysis of Ising Model Block Distribution Functions. *Z. Phys. B. Cond. Mat.* **1981**, *43*, 119-140.

(3) Rovere, M.; Hermann, D. W.; Binder, K. Block Density Distribution Function Analysis of Two-Dimensional Lennard-Jones Fluids. *Europhys. Lett.* **1988**, *6*, 585-590.

(4) Coulson, D. R.; Satek, L. C.; Grim, S. O.; Tetrakis(Triphenylphosphine)Palladium (0). *Inorg. Synth.* **1972**, *13*, 121–124.

(5) Ahmad-Junan, S. A.; Whiting, D. A. A new approach to the synthesis of peltogynoids, natural isochromeno[4,3-b]-chromenes. *J. Chem. Soc. Perkin Trans. 1* **1992**, 675–678.

(6) (a) Zhou, Q.; Carroll, P. J.; Swager, T. M. Synthesis of Diacetylene Macrocycles Derived from 1,2-Diethynyl Benzene Derivatives: Structure and Reactivity of the Strained Cyclic Dimer. *J. Org. Chem.* **1994**, *59*, 1294–1301. (b) Tahara, K.; Johnson, II, C. A.; Fujita, T.; Sonoda, M.; De Schryver, F. C.; De Feyter, S.; Haley, M. M.; Tobe, Y. Synthesis of Dehydrobenzo[18]annulene Derivatives and Formation of Self-Assembled Monolayers: Implications of Core Size on Alkyl Chain Interdigitation. *Langmuir* **2007**, *23*, 10190–10197.